Published in final edited form as:
Ann Thorac Surg. 2013 January ; 95(1): 312–318. doi:10.1016/j.athoracsur.2012.08.101.

Preclinical Study of Near-Infrared Guided Sentinel Lymph Node Mapping of the Porcine Lung

Onkar V. Khullar, MD[*,1], **Denis M. Gilmore, MD**[*,1], **Aya Matsui, MD**[2], **Yoshitomo Ashitate, MD**[2], and **Yolonda L. Colson, MD, PhD**[1]

[1]Division of Thoracic Surgery, Brigham & Women's Hospital, Boston, MA

[2]Division of Hematology/Oncology, Beth Israel Deaconess Medical Center, Boston, MA

Abstract

Background—The presence of lymph node metastasis is the most important prognostic factor in early non-small cell lung cancer. Our objective was to develop a rapid, simple, and reliable method for thoracic sentinel lymph node (SLN) identification using near-infrared fluorescence imaging and clinically available contrast agents.

Methods—Indocyanine green (ICG) was reconstituted in saline, human serum albumin, human fresh frozen plasma, and autologous porcine plasma was evaluated for optimal formulation and dosing for SLN within porcine lungs. Animals were imaged using the FLARE™ imaging system. SLN identification rate, time to identification and fluorescence intensity of the SLN, bronchus, and background were measured.

Results—SLN identification rates varied widely ranging from 33% to 100% as a function of the carrier used for ICG reconstitution. No significant difference was noted in SLN fluorescence intensity, however bronchial intensity was significantly higher with ICG:albumin, which resulted in the lowest rate of SLN identification. Subsequent evaluation with 125μM and 250μM ICG:porcine plasma resulted in identification of strongly fluorescent SLNs with identification rates of 93% and 100% and median signal-to-background ratios of 8.5 and 12.15, respectively, in <2 minutes *in situ*.

Conclusion—Near-infrared fluorescence imaging with ICG is a reliable method for SLN mapping in the lung with high sensitivity. Mixing of ICG with plasma resulted in strong SLN fluorescence signal with reliable identification rates.

Keywords

Lymph Nodes; Lung; Lung Cancer, diagnosis

To whom all correspondence should be addressed: Yolonda L. Colson, MD, PhD 75 Francis Street Division of Thoracic Surgery Boston, MA 02215 617-732-6448 FAX: ylcolson@partners.org.
*Co-first Authors

Introduction

The presence of lymph node metastases is a key prognostic factor for long-term survival in non-small cell lung cancer (NSCLC) [1]. Consequently, current staging methods for NSCLC include preoperative PET scanning and cervical mediastinoscopy to assess for metastatic disease within the mediastinum. Most surgeons will complete some degree of hilar lymphadenectomy at the time of surgery, but less than 50% of patients undergo complete lymphadenectomy to evaluate all potential sites of lymphatic spread. Sentinel lymph node (SLN) mapping offers several possible benefits over complete lymphadenectomy including improved staging and decreased morbidity by limiting nodal dissection. As a result, this technique has now become standard of care in melanoma [2] and breast cancer [3].

The need for improved staging in NSCLC is reflected in the poor 5-year survival rate of 53% and a nearly 40% recurrence rate in stage 1A disease [4], suggesting that many patients are understaged and likely harbor occult micrometastatic disease [5]. SLN mapping in NSCLC may help to focus pathologic analysis on those nodes at highest risk for containing metastatic disease. Previous attempts at SLN mapping in NSCLC have utilized isosulfan blue and/or technetium-99m [6-8]. Unfortunately these methods have been suboptimal for various reasons, including difficulty of the procedure, “shine through” of the radioisotope to nearby structures, and presence of anthracitic nodes [9]. Therefore, the current preclinical study was designed to evaluate the feasibility of near-infrared fluorescent guidance in intrathoracic SLN dissection in a large animal.

Near-infrared (NIR) fluorescence guidance has several advantages over previously utilized methods. The NIR wavelengths (700 – 1000 nm) are ideal for *in vivo* imaging as absorption, scatter, and tissue autofluorescence are all reduced within this range [10]. As a result, NIR fluorescent lymphatic tracers can be visualized up to 1cm deep in tissue allowing for intraoperative, real-time guidance of dissection [11]. Additionally, NIR light is harmless to the body, at the levels needed for fluorescence imaging, and an FDA approved NIR dye, indocyanine green (ICG), is readily available for clinical use with fluorescence further enhanced by non-covalent absorption of ICG to albumin [12,13]. Recently, ICG NIR fluorescent SLN mapping has successfully been investigated in several malignancies including breast, gastric, and skin cancers [13-18]. Therefore, the purpose of this study was to determine the feasibility and optimal dose/composition of ICG for NIR fluorescent guided SLN mapping within the lung in a large animal model.

Material and Methods

ICG Preparation

NIR fluorescence of Indocyanine green (IC-GREEN™, ICG; Akorn, Inc, Decatur, IL) is increased three-fold following noncovalent adsorption to albumin [12,13]. Therefore, ICG was resuspended in saline, 25% human serum albumin (HSA) (Baxter, Deerfield, IL), porcine plasma (PL) or human fresh frozen plasma (FFP) at a concentration of 10 μM, 125 μM or 250 μM for *in vivo* SLN mapping within the lung. PL was obtained by centrifuging fresh pig blood at 2000 rpm for 15 minutes. FFP was purchased from the Beth Israel Deaconess Medical Center (BIDMC) pharmacy.

Animal and Surgical Preparation

Female adult Yorkshire pigs (E.M. Parsons and Sons, Hadley, MA) with a mean weight of 35 kg were housed in an AAALAC-certified facility at BIDMC, staffed by full-time veterinarians. Animals were studied under the supervision of an approved institutional protocol in accordance with Institutional Animal Care and Use Guidelines and were allowed to acclimate to the animal facility for 48 hours prior to intervention. Anesthesia was induced

with 4.4 mg/kg intramuscular Telazol™ (Fort Dodge Labs, Fort Dodge, IA), and maintained with 2% isoflurane (Baxter Healthcare Corp., Deerfield, IL). Pigs were intubated with a 28Fr dual-lumen endotracheal tube via a tracheotomy. Electrocardiogram, heart rate, oxygen saturation, and body temperature were monitored during all experiments. Bilateral chest wall resections were performed to gain unobstructed imaging access to the thoracic cavity.

NIR Fluorescence Imaging System

Real-time fluorescence images were obtained using the previously described Fluorescence-Assisted Resection and Exploration for Surgery (FLARE™) open surgery imaging system in the laboratory of John Frangioni at BIDMC [13]. Color video, NIR fluorescence, and merged images were simultaneously acquired using custom software. Excitation light was produced by two wavelength-isolated excitation sources generating both white light (400-650 nm; 40,000 lux) and NIR fluorescent light (725-775 nm; 14 mW/cm^2) in a 15-cm diameter field.

NIR Fluorescence-Guided SLN Mapping

After incision, the imaging system was positioned 18” above the surgical field. 200 μL of an individual ICG formulation described above was injected 1-3 mm deep into the lung parenchyma. Initial feasibility experiments were performed with 10 μM formulations injected into right or left upper lobes (RUL or LUL), as these lobes predictably drain to the lower paratracheal, i.e. level 4 lymph nodes, and thus allow optimization of this technique [1]. Subsequent experiments utilizing 125 and 250 μM concentrations evaluated both upper and lower lobes with each animal receiving only a single injection per lobe. Fluorescence images were obtained using the FLARE™ system for 10 – 20 min post-injection with an optimal camera exposure time of 60 – 500 msec. Identified SLN(s) were resected under real-time NIR fluorescence guidance. SLN identification rate, time to identification, number of SLNs identified, and optimal camera exposure time for SLN identification were investigated.

Quantitative Assessment in NIR Fluorescence-Guided SLN Mapping

Fluorescence intensity (FI) over the SLN, bronchus, and background region of interest was quantified at the time of identification. Signal-to-background ratio (SBR) and signal-to-bronchus ratio (SBrR) were defined as SBR = (FI of SLN)/(FI of background), and SBrR = (FI of bronchus)/(FI of background) and compared between groups.

Statistical Analysis

Results were presented as median (range). The Mann-Whitney test was used to compare two groups of variables and the Kruskal-Wallis test was used to compare multiple groups with ANOVA for multiple comparisons. A p value of less than 0.05 was considered significant.

Results

Effects of 10 μM ICG Formulation on NIR Fluorescence Guided SLN Mapping in the Lung

In order to determine the optimal carrier, NIR fluorescence intensity was measured *in vitro* for 10μM ICG reconstituted with each carrier protein. On initial examination the fluorescent signal of ICG *in vitro* is greater when bound to a carrier protein, with FI increasing from 1.8 without carrier to 11.7 when bound to FFP, 10.1 bound to PL, and 9.73 bound to HSA (Figure 1). To test these combinations for maximum FI and SLN identification *in vivo*, ICG bound to HSA, PL, or FFP was injected in the right or left upper lobe of the lung. The number of SLN detected for each group is demonstrated in Table 1. Median number of SLN detected for each group was one lymph node. Time to SLN detection was 1.5 min, 3.0 min,

and 5.0 min for ICG:HSA, ICG:PL, or ICG:FFP, respectively. Figure 2 demonstrates real-time intraoperative images of lymphatic migration and SLN identification.

Signal to background ratio and signal to bronchus ratio

Given that the ability to detect SLN will be maximized when the ratio of SLN signal to background and particularly SLN signal to background signal in the bronchus is greatest, the SBR and SBrR were calculated for ICG:HSA, ICG:PL, and ICG:FFP (Figure 3). Comparing SBR among the cohorts, ICG:FFP had the highest SBR at 3.80 (range 2.27-5.31) and, although not reaching statistical significance, also exhibited the highest SBrR with a median ratio of 2.22 (range 0.41-3.85), making differentiation of SLN from the nearby bronchus the clearest. Results with ICG:PL were similar, whereas bronchial intensity was significantly higher with ICG:HSA, being brighter than the SLN signal, resulting in a SBrR of only 0.57 and making SLN identification more difficult.

Increased ICG Concentration Improves NIR Fluorescent SLN Identification

Given the similar SBR and SBrR obtained with the use of PL or FFP as the ICG carrier, ICG bound to autologous plasma (ICG:PL) was chosen as the carrier substrate for all subsequent experiments in order to minimize any potential confounding issues with the use of xenogenic blood products. To examine the impact of increasing ICG concentration on SLN visualization, 125μM and 250μM ICG:PL was utilized and resulted in rapid identification of strongly fluorescent SLNs with identification rates of 93% and 100% (Table 2). Furthermore, the median signal-to-background ratios were improved to 8.5 and 12.15, respectively, and the time to identification was < 2 minutes. NIR imaging was able to visualize the site of ICG:PL injection, the lymphatic migration pathway to the SLN and the identified SLN both *in vivo* and *ex vivo* (Figure 4). Additionally, no “shine through” effect was noted at the higher doses. The number of SLN identified, time to SLN detection, SBR and SBrR for the 125 μM and 250μM concentrations were compared, however these differences were not statistically significantly (Figure 5).

SLN location

As expected, injections in the RUL and LUL led to SLN identification in the Level 4 mediastinal station 100% of the time (16/16), skipping the nearby hilar nodes. In contrast, RLL and LLL injections predominately migrated to nearby hilar nodes (5/8 and 5/7, respectively), but exhibited migration to the mediastinum from the RLL in the residual three injections and from the LLL in two animals (Table 3). This highlights the variability of lymphatic mapping in the lung with a significant number of SLN being located within the N2 mediastinal stations and skipping traditional N1 nodes “nearest” the tumor.

Comment

In this preclinical study, we demonstrate feasibility of NIR fluorescence-guided SLN mapping using the clinically available fluorophore ICG. Previously, we have shown the utility of NIR quantum dots for intraoperative SLN mapping of the lung and pleura in swine [19,20]. Unfortunately, quantum dot fluorophores are currently not approved for human use and, given the concern of heavy metal content, will not be approved in the near future. Direct identification of SLN with ICG alone requires a large dose of ICG that carries a risk of anaphylaxis and may lead to diffuse green staining and distortion of the surgical field [21,22]. Low doses of ICG bound to plasma proteins enhance fluorescence intensity of ICG, and allow NIR detection with LED-based excitation light in a safe environment without the use of lasers, without radiation risk, and without distortion of the surgical field. Using a large animal model, the current study demonstrates that NIR fluorescence imaging with ICG is an effective, simple, and rapid method for SLN mapping in the lung. Furthermore, a

dramatic enhancement of ICG fluorescence is seen when bound with plasma proteins, resulting in protein concentration-dependent enhancement in SLN fluorescence with low background secondary to improved quantum yield and SLN retention in swine.

Our comparison of equivalent *in vivo* doses of ICG bound to human serum albumin, autologous porcine plasma or human fresh frozen plasma for SLN mapping, demonstrated no significant difference in the signal of ICG as a function of the type of carrier protein. Further dose escalation using 125 uM and 250 uM ICG:PL demonstrated a dose dependent increase in the SLN identification rate, SBR, and SBrR, with a 100% SLN identification rate in all four lobes with the 250 uM cohort. Based on this data, ICG:PL appears ideal for NIR-image guided SLN mapping since NIR fluorescence of ICG is increased both *in vivo* and *ex vivo*. Although ICG is considered safe and clinically used at intravenous doses of 0.5-2.0 mg/kg in hepatic and cardiac function testing, there is a risk of anaphylaxis [23]. The prolonged effects of high dose ICG are unknown and therefore minimizing the necessary ICG dose by coupling to plasma proteins may be a safer alternative for patients requiring lymphatic mapping. Therefore, to minimize toxicity, the current study injects ICG within the parenchyma and uses doses hundreds of times lower at only 2, 25 and 50 μg. As a result, blood levels would be well below clinically utilized levels.

Lymphatic drainage patterns of the lung are difficult to predict with the lymphatic drainage in human lung being mapped to up to 13 common lymph node stations. Lymphatic drainage is also highly variable among tumors with 20% of SLN skipping to the N2 nodes in the mediastinum [24,25]. As a result, metastatic mediastinal disease may be missed, resulting in the under treatment of patients and a significant decrease in overall survival. In the current study, lymphatic drainage from both the right and left upper lobes predictably drained to the level 4 mediastinal lymph node station in all cases, whereas only five of fifteen injections (33%) in the lower lobes resulted in mediastinal SLN identification. Based on this data, the SLN bypassed hilar nodes and skipped to the mediastinum a significant amount of time, supporting what is clinically manifest as skip metastases.

There are several limitations to this study. First, in the current feasibility study the chest wall was resected to allow maximum access for imaging given the limited visibility of a thoracotomy in a pig model, in order to allow determination of optimal dosing and imaging technique. Based on these results we have initiated an early ongoing clinical trial in which our preliminary data has established that standard thoracotomy without chest wall resection is sufficient for imaging with the FLARE™ system and that videoscopic imaging is feasible using the Novadaq NIR videoscope, such that we do not anticipate imaging access to ultimately prevent clinical translation of this technology. Second, porcine anatomy, while similar to human anatomy is not identical as pigs lack intralobar lymph nodes [26]. Although we expect this technology to still be effective at identifying any SLN at these stations, intralobar nodes could not be evaluated in the current study. Third, the absence of a large animal lung cancer model prevented the initial assessment of NIR technology in the setting of tumor and lymphatic involvement. However, it did permit initial safety studies and the upscale of the technology from rodents to animals “the size of humans” which was critical for the initial translation of NIR imaging into humans. Differences in lymphatic anatomy, physiology, and biology in the setting of lung cancer patients will be important parameters to be determined within the context of our ongoing phase I/II clinical trial. Finally, as there is no current clinically acceptable method for accurate SLN detection within the lung it is difficult to determine sensitivity, specificity, and accuracy against a non-existent “gold standard.” NIR SLN identification has been shown to have similar accuracy compared to SLN lymphoscintigraphy in patients with breast cancer [13-15].

In summary, this preclinical study demonstrates that ICG coupled with plasma proteins increases NIR fluorescence for SLN identification in a swine lung model at markedly lower ICG doses than used for other clinical interventions. Given the safety and feasibility demonstrated in this large animal study, NIR guided SLN mapping may prove to be effective in patients with surgically resectable NSCLC in the identification of lymph nodes at greatest risk for metastases thus permitting further analysis of these nodes and more accurate staging. Based on this pre-clinical study, the optimal ICG dosing and technique in patients with early stage surgically resectable lung cancer is currently the focus of a phase I clinical trial.

Acknowledgments

This work was supported by the National Institutes of Health RO1-CA-131044-01A1 and the Thoracic Surgery Foundation for Research and Education Research Fellowship. The authors would like to acknowledge John Frangioni, MD, PhD for providing the animals and FLARE imaging platform used in this study.

Abbreviations and Acronyms

AAALAC	Association for Assessment and Accreditation of Laboratory Animal Care
BIDMC	Beth Israel Deaconess Medical Center
FFP	human fresh frozen plasma
FI	fluorescence intensity
FLARE	Fluorescence-Assisted Resection and Exploration for Surgery
HSA	human serum albumin
ICG	indocyanine green
LLL	left lower lobe
LN	lymph node
LUL	left upper lobe
NIR	near infrared
NSCLC	non-small cell lung cancer
PL	porcine plasma
RLL	right lower lobe
RUL	right upper lobe
SBR	signal-to-background ratio
SBrR	signal-to-bronchus ratio
SLN	sentinel lymph node

References

1. Mountain CF, Dresler CM. Regional lymph node classification for lung cancer staging. Chest. 1997; 111:1718–1723. [PubMed: 9187199]
2. Morton DL, Cochran AJ, Thompson JF, et al. Sentinel node biopsy for early-stage melanoma: accuracy and morbidity in MSLT-I, an international multicenter trial. Ann Surg. 2005; 242:302–311. [PubMed: 16135917]
3. Krag D, Weaver D, Ashikaga T, et al. The sentinel node in breast cancer--a multicenter validation study. N Engl J Med. 1998; 339:941–946. [PubMed: 9753708]

4. Howlader, N.; Noone, AM.; Krapcho, M., et al. Seer Cancer Statistic Review, 1975-2008. National Cancer Institute; Bethesda, MD: 2011. Available at http://seer.cancer.gov/csr/1975_2008/. Posted to the SEER web site
5. Chen ZL, Perez S, Holmes EC, et al. Frequency and distribution of occult micrometastases in lymph nodes of patients with non-small-cell lung carcinoma. J Natl Cancer Inst. 1993; 85:493–498. [PubMed: 7680382]
6. Little AG, DeHoyos A, Kirgan DM, Arcomano TR, Murray KD. Intraoperative lymphatic mapping for non-small cell lung cancer: the sentinel node technique. J Thorac Cardiovasc Surg. 1999; 117:220–224. [PubMed: 9918960]
7. Schmidt FE, Woltering EA, Webb WR, Garcia OM, Cohen JE, Rozans MH. Sentinel nodal assessment in patients with carcinoma of the lung. Ann Thorac Surg. 2002; 74:870–874. [PubMed: 12238853]
8. Liptay MJ, D'amico TA, Nwogu C, et al. Intraoperative sentinel node mapping with technitium-99 in lung cancer: results of CALGB 140203 multicenter phase II trial. J Thorac Oncol. 2009; 4:198–202. [PubMed: 19179896]
9. Nwogu C. Sentinel node and positron emission tomography mapping in lung cancer. Semin Thorac Cardiovasc Surg. 2010; 21:323–326. [PubMed: 20226345]
10. Khullar O, Frangioni JV, Grinstaff M, Colson YL. Image-guided sentinel lymph node mapping and nanotechnology-based nodal treatment in lung cancer using invisible near-infrared fluorescent light. Semin Thorac Cardiovasc Surg. 2010; 21:309–315. [PubMed: 20226343]
11. Tanaka E, Choi HS, Fujii H, Bawendi MG, Frangioni JV. Image-guided oncologic surgery using invisible light: completed pre-clinical development for sentinel lymph node mapping. Ann Surg Oncol. 2006; 13:1671–1681. [PubMed: 17009138]
12. Ohnishi S, Lomnes SJ, Laurence RG, Gogbashian A, Mariani G, Frangioni JV. Organic alternatives to quantum dots for intraoperative near-infrared fluorescent sentinel lymph node mapping. Mol Imaging. 2005; 4:172–181. [PubMed: 16194449]
13. Troyan S, Kianzad V, Gibbs-Strauss S, et al. The FLARE™ intraoperative near-infrared fluorescence imaging system: A first-in-human clinical trial in breast cancer sentinel lymph node mapping. Ann Surg Oncol. 2009; 16:2943–2952. [PubMed: 19582506]
14. Mieog JS, Troyan SL, Hutteman M, et al. Towards optimization of imaging system and lymphatic tracer for near-infrared fluorescent sentinel lymph node mapping in breast cancer. Ann Surg Oncol. 2011; 18:2483–2491. [PubMed: 21360250]
15. Hojo T, Nagao T, Kikuyama M, Akashi S, Kinoshita T. Evaluation of sentinel node biopsy by combined fluorescent and dye method and lymph flow for breast cancer. Breast. 2010; 19:210–213. [PubMed: 20153649]
16. Crane LM, Themelis G, Pleijhuis RG, et al. Intraoperative multispectral fluorescence imaging for the detection of the sentinel lymph node in cervical cancer: a novel concept. Mol Imaging Biol. 2011; 13:1043–1049. [PubMed: 20835767]
17. Schaafsma BE, Mieog JSD, Hutteman M, et al. The clinical use of indocyanine green as a near-infrared fluorescent contrast agent for image-guided oncologic surgery. J Surg Oncol. 2011; 104:323–332. [PubMed: 21495033]
18. Fujisawa Y, Nakamura Y, Kawachi Y, Otsuka F. Indocyanine green fluorescence-navigated sentinel node biopsy showed higher sensitivity than the radioisotope or blue dye method, which may help to reduce false-negative cases in skin cancer. J Surg Oncol. 2012; 106:41–45. [PubMed: 22252373]
19. Soltesz EG, Kim S, Laurence RG, et al. Intraoperative sentinel lymph node mapping of the lung using near-infrared fluorescent quantum dots. Ann Thorac Surg. 2005; 79:269–277. [PubMed: 15620956]
20. Parungo CP, Colson YL, Kim SW, et al. Sentinel lymph node mapping of the pleural space. Chest. 2005; 127:1799–1804. [PubMed: 15888861]
21. Ishikawa K, Yasuda K, Shiromizu A, Etoh T, Shiraishi N, Kitano S. Laparoscopic sentinel node navigation achieved by infrared ray electronic endoscopy system in patients with gastric cancer. Surg Endosc. 2007; 21:1131–1134. [PubMed: 17180275]

22. Yamashita S, Tokuishi K, Miyawaki M, et al. Sentinel node navigation surgery by thoracoscopic fluorescence imaging system and molecular examination in non-small cell lung cancer. Ann Surg Onc. 2012; 19:728–733.

23. Henschen S, Busse MW, Zisowsky S, Panning B. Determination of plasma volume and total blood volume using indocyanine green: A short review. J Med. 1993; 24:10–27. [PubMed: 8501401]

24. Takizawa T, Terashima M, Koike T, et al. Lymph node metastasis in small peripheral adenocarcinoma of the lung. J Thorac Cardiovasc Surg. 1998; 116:276–280. [PubMed: 9699580]

25. Kubuschok B, Passlick B, Izbicki JR, Thetter O, Pantel K. Disseminated tumor cells in lymph nodes as a determinant for survival in surgically resected non–small cell lung cancer. J Clin Oncol. 1999; 17:19–24. [PubMed: 10458213]

26. Riquet M, Souilamas R, Hubsch JP, Briere J, Colomer S, Hidden G. Lymphatic drainage of heart and lungs: comparison between pig and man. Surg Radiol Anat. 2000; 22:47–50. [PubMed: 10863747]

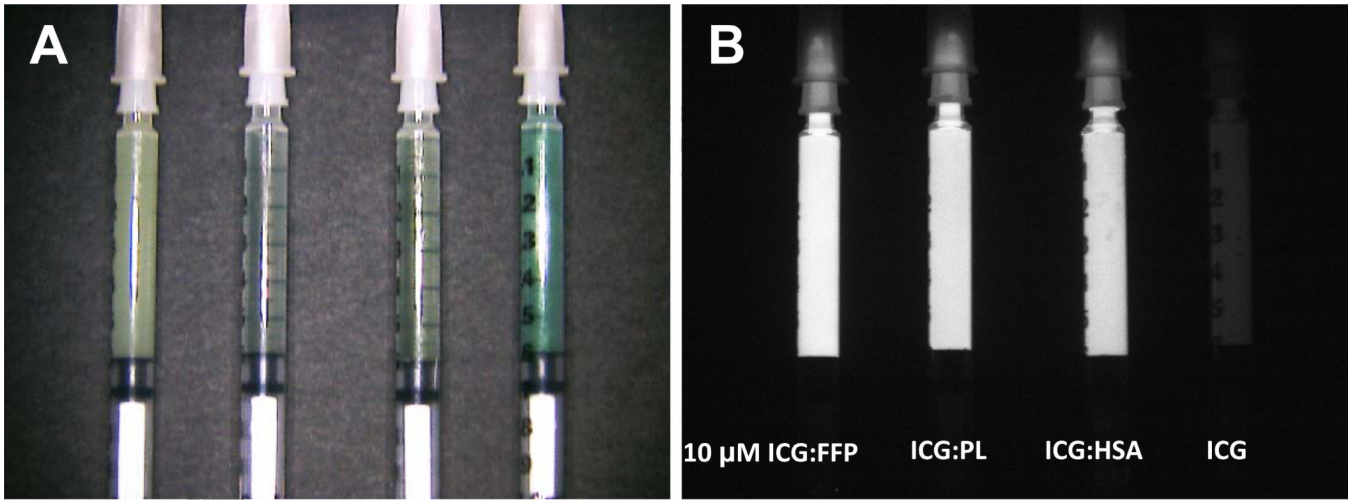

Figure 1. Optical properties of ICG solutions in conjunction of different proteins

Shown are the color image (A) and NIR fluorescence image (B) of ICG:FFP, ICG:PL, ICG:HSA, and ICG along without a carrier protein (left to right) packed in 1 cc tuberculin syringe. SBR for each solution was 11.7, 10.1, 9.73, and 1.8, respectively.; ICG: Indocyanine Green; FFP: human fresh frozen plasma; HSA: human serum albumin; PL: porcine plasma.

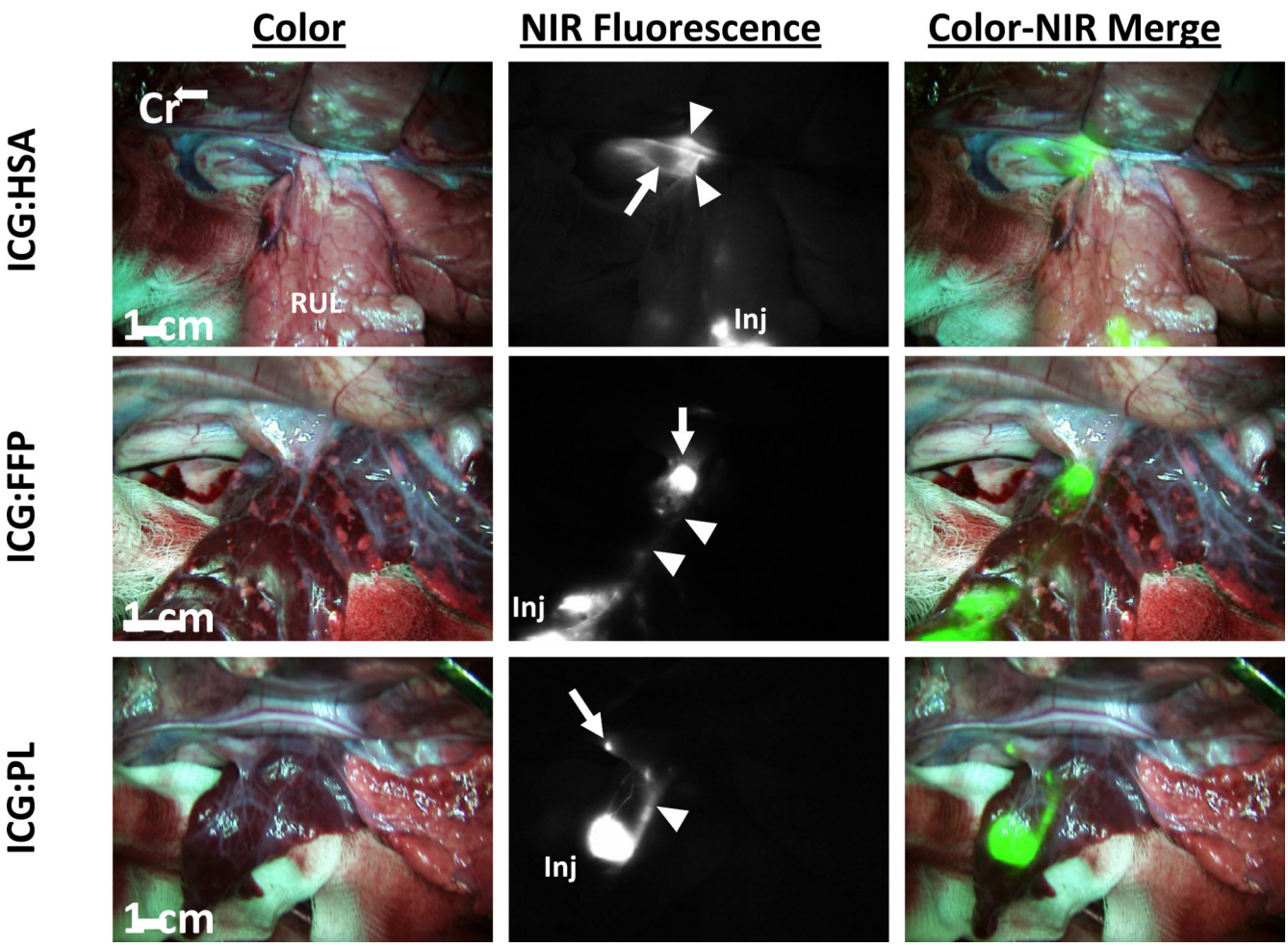

Figure 2. Successful visualization of 10uM of ICG coupled with human serum albumin (ICG:HSA), fresh frozen plasma (ICG:FFP), or porcine plasma (ICG:PL)

The first column represents the surgical field as seen with the human eye. The second column is an NIR image of the surgical field with fluorescence. The third column is a merged overlay of the white and NIR images pseudo-colored green demonstrating visualization of the injection site, lymphatic pathway and SLN. Cr: cranial; ICG: Indocyanine Green; Inj: injection; FFP: human fresh frozen plasma; HSA: human serum albumin; PL: porcine plasma; Arrow: sentinel lymph node, Arrowhead: bronchus

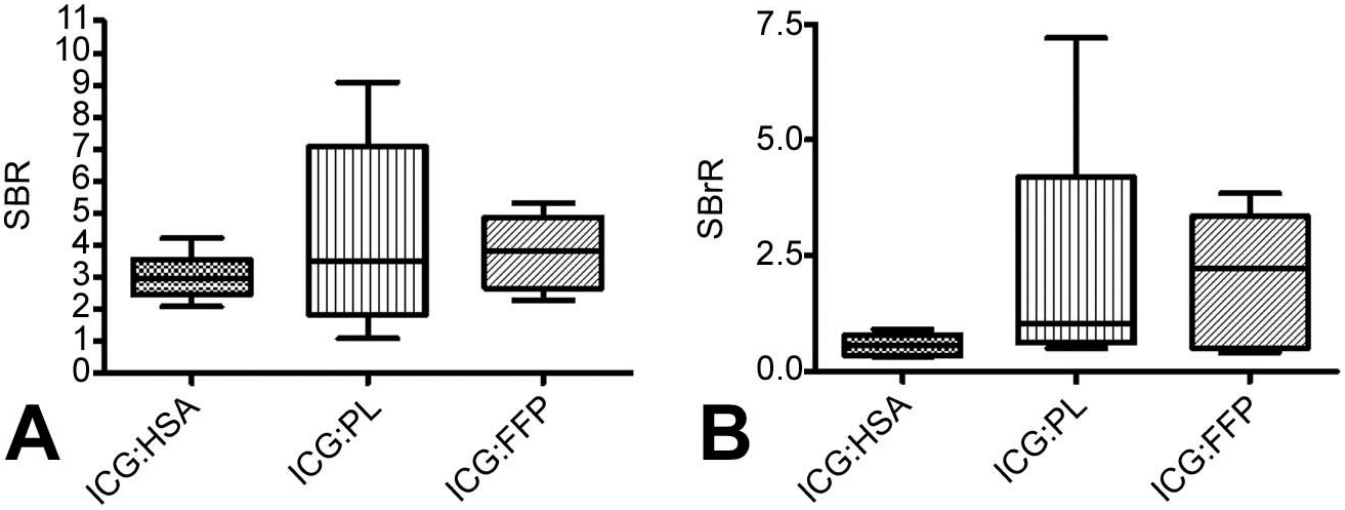

Figure 3. *In Vivo* signal intensity of ICG bound to proteins

In vivo Signal-to-Background (SBR) (A) and Signal-to-Bronchus Ratio (SBrR) (B) were calculated for ICG bound to each protein. There was no significant difference in the SBR or SBrR for ICG bound to any of the plasma proteins. ICG: Indocyanine Green; FFP: human fresh frozen plasma; HSA: human serum albumin; PB: purified human serum albumin; PL: porcine plasma.

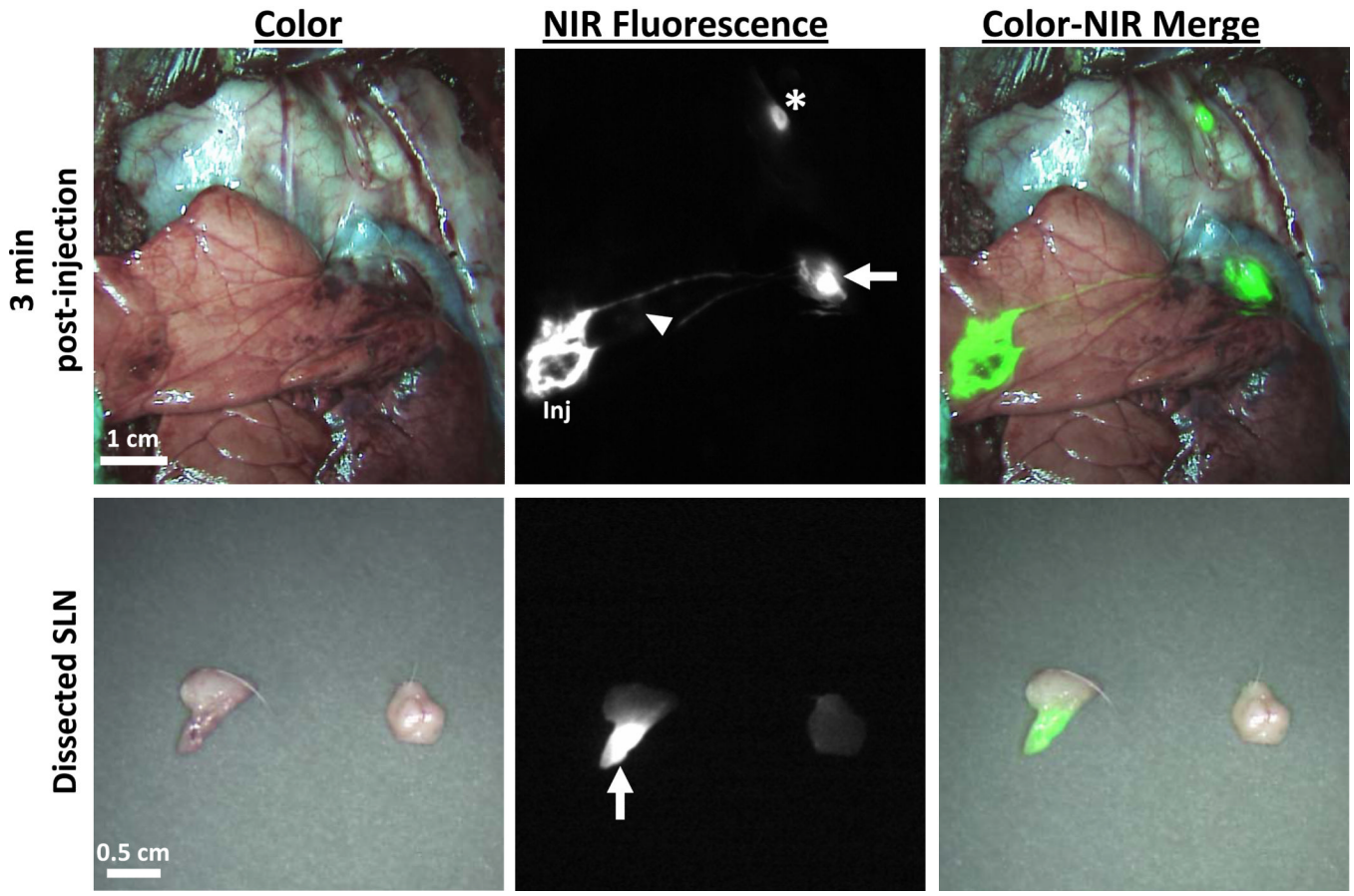

Figure 4. *In vivo* and Ex Vivo identification of the SLN using 250uM of ICG:PL

The first row demonstrates *in vivo* NIR imaging of the injection site, lymphatic migration and SLN identification. Following resection of the SLN, *ex vivo* NIR fluorescence imaging confirms uptake of ICG within the lymph nodes seen in the second row. Arrow: primary SLN; Arrowhead: bronchus; Star: secondary lymph node.

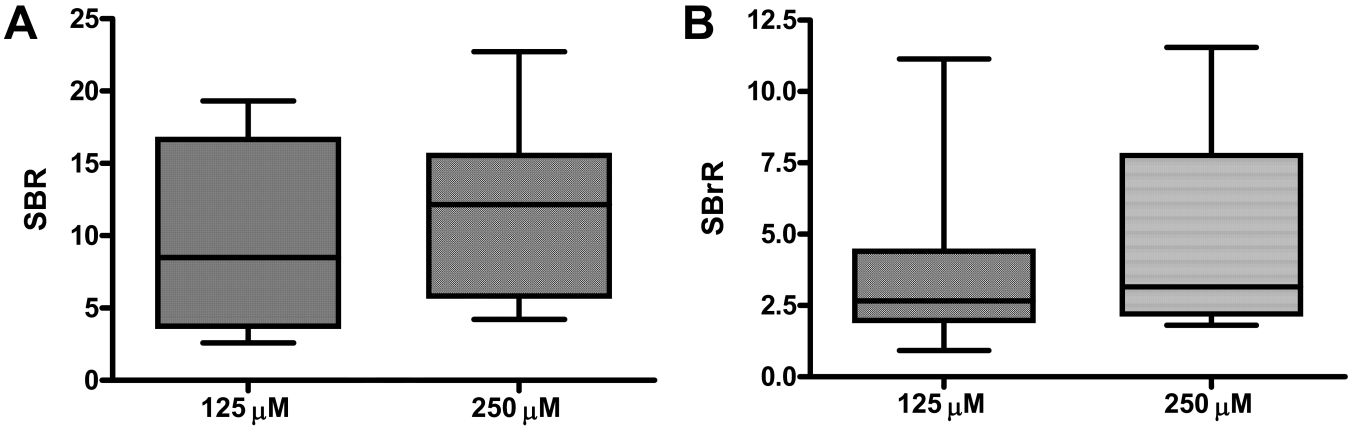

Figure 5. Dose dependent increase in SBR and SBrR

Following *in vivo* injection of 200 uL of 125 uM or 250 uM bound to porcine plasma, the SBR and SBrR were calculated. There is a dose dependent increase in both SBR and SBrR when compared with the 10 uM dose. (A) Signal-to-Background Ratio; (B) Signal-to-Bronchus Ratio.

Table 1

Effects of 10 μM ICG Formulation on NIR Fluorescence Guided SLN Mapping in the Lung

Contrast Agent	Total # Injections	SLN Detected	Median # of SLN Identified (range)	Time to SLN Identification (min) (range)	Optimal Camera Exposure Time (msec) (range)	SBR (range)	SBrR (range)
ICG:HSA	6	2/6	1 (1 - 4)	1.5 (1 - 2)	150 (150)	2.96 (2.07 - 4.21)	0.57 (0.31 - 0.91)
ICG:PL	8	7/8		3.0 (1 - 10)	150 (60 - 250)	3.49 (1.07 - 9.09)	1.05 (0.51 - 7.20)
ICG:FFP	8	8/8	1 (1 - 2)	5.0 (1 - 10)	225 (67 - 500)	3.80 (2.27 - 5.31)	2.22 (0.41 - 3.85)

FFP: human fresh frozen plasma; HSA: human serum albumin; ICG: Indocyanine Green; PL: porcine plasma; SLN: sentinel lymph node; SBR: signal-to-background ratio; SBrR: signal-to-bronchus ratio

Table 2

Increased ICG Concentration Improves NIR Fluorescent SLN Identification

ICG Concentration	Injection Site	Total # Injections	SLN Detected	Median # SLN Identified (range)	Time to SLN Identification (min) (range)	Optimal Camera Exposure Time (msec) (range)	SBR (range)	SBrR (range)
125 μM	RUL	4	4/4	1 (1-2)	0.50 (0.333 - 0.667)	70 (30 - 200)	11.85 (3.00 - 17.86)	3.53 (0.92 - 3.93)
	RLL	4	4/4	1 (1 - 4)	2.25 (0.75 - 10)	100 (60 - 100)	7.56 (3.72 - 8.82)	2.65 (1.39 - 4.88)
	LUL	4	4/4	1 (1 - 2)	0.42 (0.25 - 0.75)	70 (30 - 250)	10.49 (2.59 - 19.33)	5.44 (2.19 - 11.14)
	LLL	3	2/3	1 (0 - 1)	2 (2)	100 (100)	10.93 (5.77 - 16.09)	1.97 (1.9 - 2.04)
	Total/Median	15	14/15	1	0.71	70	8.5	2.67
250 μM	RUL	4	4/4	2 (1 - 2)	0.42 (0.167 - 1)	30 (30 - 60)	13.86 (8.07 - 22.69)	6.31 (2.22 - 8.94)
	RLL	4	4/4	1.5 (1 - 2)	2.50 (2 - 4)	80 (30 - 100)	10.01 (4.88 - 18.92)	2.14 (1.81 - 7.24)
	LUL	4	4/4	1.5 (1 - 2)	0.50 (0.167 - 3)	60 (30 - 150)	9.91 (4.22 - 22.71)	8.28 (3.11 - 11.55)
	LLL	4	4/4	1 (1)	6.50 (1.5 - 10)	80 (60 - 150)	11.09 (5.71 - 14.71)	3.01 (2.01 - 3.15)
	Total/Median	16	16/16	1	1.75	60	12.15	3.15

FFP: human fresh frozen plasma; ICG: Indocyanine Green; LLL: left lower lobe; LUL: left upper lobe; NPB: non-purified human serum albumin; PL: porcine plasma; SBR: signal-to-background ratio; SBrR: signal-to-bronchus ratio; SLN: sentinel lymph node; RLL: right lower lobe; RUL: right upper lobe

Ann Thorac Surg. Author manuscript; available in PMC 2014 January 01.

Table 3

SLN Location

		Hilar	Mediastinal	
Injection Site	**Number of Injections**	**Level 10 SLN**	**Level 4 SLN**	**Level 7 SLN**
RUL	8	0	8	0
RLL	8	5	1	2
LUL	8	0	8	0
LLL	7	5	0	1
Total	**31**	**10**	**17**	**3**

LLL: left lower lobe; LUL: left upper lobe; RLL: right lower lobe; RUL: right upper lobe, SLN: sentinel lymph node